Rochester Institute of Technology

RIT Digital Institutional Repository

6-5-2020

Low frequency cyclical potentials for fine tuning nonlinear electrokinetic separations

Cody Justice Lentz
cjl5831@rit.edu

Follow this and additional works at: https://repository.rit.edu/theses

Low frequency cyclical potentials for fine tuning

nonlinear electrokinetic separations

By:

Cody Justice Lentz

Low frequency cyclical potentials for fine tuning

nonlinear electrokinetic separations

By:

Cody Justice Lentz

A thesis submitted in partial fulfillment of the requirements for the

degree of Master of Science in Mechanical Engineering

Department of Mechanical Engineering

Kate Gleason College of Engineering

Approved by:

_____
Dr. Blanca Lapizco-Encinas, Professor   Date
Thesis Advisor, Department of Biomedical Engineering

_____
Dr. Michael Schertzer, Associate Professor   Date
Committee Member, Department of Mechanical Engineering

_____
Dr. Michael Schrlau, Associate Professor   Date
Committee Member, Department of Mechanical Engineering

_____
Dr. Alan Nye, Professor   Date
Department Representative, Department of Mechanical Engineering

Abstract:

This work has shown a novel method for the separation of particles inside a nonlinear EK device using low frequency cyclical signals. The utility of this method was demonstrated by successfully separating micron sized polystyrene particles based on differences in particle size (2 µm vs. 5.1 µm) and by differences in particle charge (19 vs. 60 mv). In order to discover a usable signal for separation, a custom Matlab program was developed to simulate particle migration inside the device. The custom program utilized data from finite element analysis of the electric field in the device using the COMSOL Multiphysics program. After successfully separating particle using this method, it was discovered that the more likely force present in the system was not DEP, as was previously assumed, but rather nonlinear electrophoresis. The knowledge of this phenomena was implemented into the custom Matlab program. However, the method previously created for determining μ_{DEP} was not usable for the determination of $\mu_{EP}^{(3)}$. In light of this, the second part of this study was preformed to determine a useable method for determining $\mu_{EP}^{(3)}$. Three methods were developed and tested on one particle type. The best method from these three methods were selected and used for the determination of $\mu_{EP}^{(3)}$ for four distinct particle types. These $\mu_{EP}^{(3)}$ values were then compared to $\mu_{EP}^{(3)}$ values derived from the latest model for nonlinear EP in systems similar to those used in this study [1]. The methodology developed in this work could have applications in the development of methods and devices which could separate micron-sized bioparticles such as yeast and bacteria.

Acknowledgments

I would like to thank Dr. Blanca Lapizco-Encinas and the microscale bioseparations lab for providing an opportunity to conduct this research as well as help throughout. I would also like to thank Samuel Hidalgo for conducting much of the first half of this work with me as well as teaching me many techniques necessary for this work. I would also like to thank Sofia Antunez Vela and Adriana Coll De Peña for their help with the second half of this work. I would also like to thank Sofia Antunez Vela, Adriana Coll De Peña, Samuel Hidalgo, Abbi Miller, Nicole Hill, and Johnathan Chu for being the best lab mates I could ask for. I would also like to thank my soon to be wife Erin Petrillose as well as my family, Brian, Cheryl, Melissa, and Katie, for their love and support all these years. I would especially like to thank my mom for teaching me before college, and to whom I owe my love of learning.

Table of contents

List of figures

List of tables

Nomenclature

POC	Point-of-care
EK	Electrokinetics
EOF	Electroosmotic flow
EP	Electrophoresis
DEP	Dielectrophoresis
EDL	Electrical double layer
eDEP	Electrode based dielectrophoresis
iDEP	Insulator based dielectrophoresis
$\mu_{EP}^{(1)}$	Linear electrophoretic mobility
ζ	Zeta potential

ε	Permittivity
η	Dynamic viscosity
μ_{EO}	Electroosmotic mobility
μ_{DEP}	Dielectrophoretic mobility
r_p	Particle radius
f_{CM}	Clausius-Mossotti factor
σ	Conductivity
K_s	Stern layer conductance
μ_{EK}	Electrokinetic mobility
$\mu_{EP}^{(3)}$	Nonlinear electrophoretic mobility
φ_T	Thermal voltage

Du	Dukhin number
Bi	Bikerman number
λ	Debye length
k_b	Boltzman constant
T	Absolute temperature
e	Charge of an electron
R_{gas}	Gas constant
F_c	Faraday constant
Z	Electrolyte valance
c	Molar concentration of an electrolyte
$\alpha^{\pm}$	Ionic drag coefficients

$D_{\pm}$	Ion diffusivity
E_{EEC}	Electrokinetic equilibrium condition

1.0 Introduction

1.1 Background

Microfluidics is an area of growing interest which uses small volumes of liquid to create platforms that are inexpensive, portable, and/or exploit unique phenomena. Microfluidics are particularly interesting for the analysis of bioparticles in a portable point-of-care (POC) diagnostic device. Because the device dimensions are small, the required sample volumes for microfluidic diagnostic devices could be much smaller than normal and the detection limit could be as low as a single molecule or cell [2–4]. The size, shape, and electrical phenotype of a bioparticle can provide insight into the strain, pathogenicity, and antibiotic resistance of that particle [5,6].

One of the unique phenomena only significant in microfluidics is electrokinetics (EK) which is the movement of fluid or particles due to an applied electric field. The specific EK phenomena discussed in this study are electroosmotic flow (EOF), electrophoresis (EP), and dielectrophoresis (DEP). Forces due to EP and DEP depend on the electrical phenotype, as well as the size and shape, of a bioparticle which allows EK microfluidic devices to distinguish between different bioparticles for analysis or purification. Devices utilized EOF and EP have had widespread adoption in the form of capillary electrophoresis [7]. Devices employing DEP forces have had some adoption [8,9] in commercial devices.

The velocity of a particle due to EOF and EP are linearly related to the magnitude of the electric field and are therefore commonly referred to as linear EK. The EOF phenomena is created because when an ionic solution comes into contact with a charged surface a layer of ions builds up along the surface (represented by "+" in Fig. 1a) known as the electrical double layer (EDL). When

an electric field is applied the ions along the surface move and the fluid velocity propagates

throughout the entire channel (see Fig. 1a). In the case of this work the channel walls are negatively

charged and majority of the EDL ions are positive, causing the EOF to go in the positive electric

field direction. One of the most useful aspects of EOF is extremely flat velocity profile it generates

(see Fig. 1a) which is created because the force generating fluid movement is applied along the

surface so there is no parabolic profile caused by a no-slip boundary condition [10]. The velocity of

a particle due to EP is caused by the coulombic force acting on the charged surface on the particle

[10]. Because the charged particles are suspended in an ionic solution the particles build up an EDL

as shown in Figure 1b which at higher electric fields can change shape and changes EP velocity

[1,11,12].
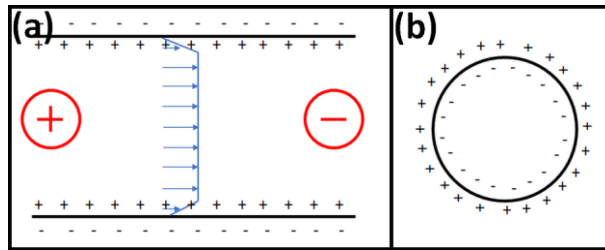
Figure 1: (**a**) Cartoon representation of EOF of a negatively charged surface with electric field going left to right. Positive ions in EDL are represented by "+" and velocity profile is shown in blue. The nonconstant part of the velocity profile is exaggerated for visibility. (**b**) Cartoon representation of EDL for negatively charged particle. Positive ions in EDL are represented by "+".

The phenomenon of DEP is present when a particle is polarized due to a distorted electric

field having a larger magnitude on one end of the particle than the other. Devices employing DEP

fall into two main categories based on how the electric field is distorted: electrode based (eDEP)

(see Fig. 2a) which rely on the shape or position of the electrodes to cause a distorted field and

insulator based (iDEP) (see Fig. 2b) which utilizes insulating structures to change the cross-sectional area the field passes through. The majority of eDEP systems are AC systems with frequencies near or above 1 kHz [8] while iDEP systems are being studied using AC and DC signals [13]. The main form of particle separation using AC signals is applying a certain frequency such that one particle moves towards areas of changing electric field while the other particles move away from areas of changing electric field. This is possible because for most particles the Clausius-Mossotti factor (f_{CM}) changes sign, causing the DEP force to change direction (Eqn. 4) at a frequency known as the crossover frequency. Systems using DC signals, on the other hand, generally rely on the magnitude of the DEP force to differ between particle types (usually due to size differences) or have similar DEP forces and utilize differences in EP to DEP force ratios.
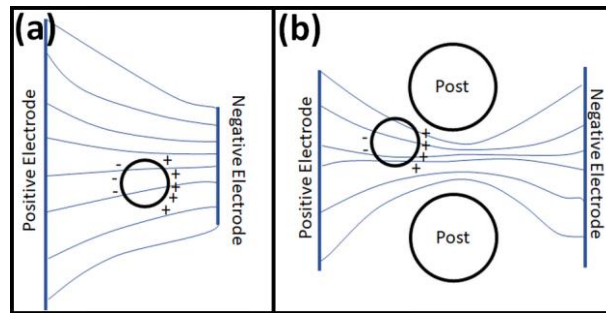
Figure 2: (**a**) Cartoon representation of eDEP with spatial nonconformity caused by differing sizes in electrodes. (**b**) Cartoon representation of iDEP with spatial nonconformity caused by the area for the electric field to pass though decreasing between the posts. The particle is experiencing DEP forces as it enters the constriction.

Recently, research [14,15] has shown that much of what was previously thought of as DEP forces in DC iDEP devices are actually nonlinear EP forces. Nonlinear EP or EP of the second kind is a component of the EP velocity of the particles which is proportional to the electric field cubed

3

[1,12]. This term can usually be ignored because normal EP experiments have low electric field magnitudes. However, in many iDEP devices the modest electric field is increased sharply, previously thought to induce DEP, but now thought to increase the electric field to a magnitude where EP of the second kind is significant.

1.2 Literature Review

1.2.1 Linear Electrokinetics

When a particle is in an ionic solution and an electric field is applied the coulombic force causes the particle to move with a velocity shown below [10,16].

$$\vec{v}_{EP}^{(1)} = \mu_{EP}^{(1)} \vec{E} = \frac{-\varsigma_P \varepsilon_m}{\eta} \vec{E} \tag{1}$$

Here $\mu_{EP}^{(1)}$ is the linear EP mobility, ς_P is the particle zeta potential, ε_m is the media permittivity, η is the permittivity, and $\vec{E}$ is the electric field.

A particle in a channel with EOF will have a velocity described below [10,16].

$$\vec{v}_{EO} = \mu_{EO}\vec{E} = \frac{-\varsigma_W \varepsilon_m}{\eta} \vec{E} \tag{2}$$

Here μ_{EO} is the EOF mobility and ς_W is the wall zeta potential.

The full linear EK particle velocity is shown below where μ_{EK} is the linear EK mobility.

$$\vec{v}_{EK} = \vec{v}_{EP}^{(1)} + \vec{v}_{EO} = \mu_{EP}^{(1)} \vec{E} + \mu_{EO}\vec{E} = \mu_{EK}\vec{E} = -\frac{\varepsilon_m(\varsigma_W - \varsigma_P)}{\eta} \vec{E} \tag{3}$$

1.2.3 Dielectrophoresis

Particles experiencing DEP are polarized, as shown in Fig. 2, cause the particle to move with the

following velocity [10,16].

$$\vec{v}_{DEP} = \mu_{DEP}\nabla E^2 = \frac{r_p^2 \varepsilon_m}{3\eta} Re[f_{CM}]\nabla E^2 \qquad (4)$$

where r_p is the radius of the particle, ∇E^2 is the gradient of the electric field squared and $Re[f_{CM}]$

is the real part of the Clausius-Mossotti factor. For frequencies below 100 kHz $Re[f_{CM}]$ can be

assumed to be [17]:

$$f_{CM} = \left(\frac{\sigma_p - \sigma_m}{\sigma_p + 2\sigma_m}\right) \qquad (5)$$

where σ is the real conductivity of the particle and the medium. All particles in this study exhibited

negative DEP, meaning that the particles move in the opposite direction of ∇E^2. The particle

conductivity (σ_p) depends on the conductivity of the bulk material (σ_b), and the surface

conductance (K_s) [18]:

$$\sigma_p = \sigma_b + 2\frac{K_s}{r_p} \qquad (6)$$

The overall particle velocity, assuming only linear EK and DEP, is given by the equation [19–21]:

$$\vec{v}_P = \mu_{EK}\vec{E} + \mu_{DEP}\nabla E^2 = -\frac{\varepsilon_m\left(\zeta_{wall} - \zeta_{particle}\right)}{\eta}\vec{E} + \frac{r_p^2 \varepsilon_m}{3\eta} Re[f_{CM}]\nabla E^2 \qquad (7)$$

where μ_{EK} and μ_{dep} are the EK and DEP mobilities, respectively. Particle trapping occurs when

$\vec{v}_P = 0$, and Eqn. 7 can be rearranged to estimate μ_{DEP} [22]:

$$\mu_{DEP} = \frac{\mu_{EK}|\vec{E}|}{|\nabla E^2|} \tag{8}$$

1.2.4 Nonlinear Electrophoresis

While EP velocity at low electric field magnitudes is linearly related to the electric field magnitude (Eqn. 1), however, at higher electric field magnitudes, defined by the voltage drop across a particle being comparable to the thermal voltage, the EP velocity is dependent on a linear and a cubic term. [1,12,15,23] The formulation of this cubic term below is the dimensionalized form of Schnitzer et al. [1].

$$\vec{v}_{EP}^{(3)} = \mu_{EP}^{(3)} \left(\vec{E} \cdot \vec{E}\right)\vec{E} = \frac{-r_p^2 \, \varepsilon_m}{\eta \, \varphi_T} \, f(\text{Du}, \zeta_0, \alpha, \dot{\alpha}) \left(\vec{E} \cdot \vec{E}\right)\vec{E} \tag{9}$$

Where r_p is the particle radius, φ_T is the thermal voltage, and

$$f(\text{Du}, \zeta_0, \alpha, \dot{\alpha}) = \frac{\text{Du}(k_0 + k_1\text{Du} + k_2\text{Du}^2 + k_3\text{Du}^4 + k_5\text{Du}^5)}{840(1+2\text{Du})^4(1+4\text{Du})(1+6\text{Du})} \tag{10}$$

where the k values are dependent on particle charge and the suspending media, α and $\dot{\alpha}$ are modified ion drag coefficients, and ζ_0 is a nondimensional form of particle zeta potential. Equations for all of these are below (Eqn. 13-24). Additionally, the modified Dukhin number (Du) is defined by the following.

$$Du = \text{Bi}(1 + 2\alpha^-) \tag{11}$$

With the Bikerman number (Bi) formulated as follows:

$$Bi = \frac{\lambda \, \zeta_p}{r_p \, \varphi_T} \tag{12}$$

With λ being the Debye length. In addition to dimensionalizeing all of the terms in from Schnitzer et al., [1] particle surface conductance terms were modified using the Grahame equation [24] so that particle zeta potentials could be used.

The thermal voltage is defined by:

$$\varphi_T = \frac{k_b T}{e} \tag{13}$$

with k_b as the Boltzman constant, T being the temperature, and e is the charge of an electron. The Debye length is defined as:

$$\lambda = \sqrt{\frac{\varepsilon_m R_{gas} T}{8 \pi F_c^2 \sum cZ^2}} \tag{14}$$

with R_{gas} being the gas constant, F_c being the Faraday constant, c being the molar concentration of an electrolyte, and Z being the valance of that electrolyte.

The nondimensionalized zeta potential is defined as follows.

$$\zeta_0 = 2\ln\left(\frac{\zeta_p}{\varphi_T}\right) \tag{15}$$

The modified ionic drag coefficents are defined as:

$$\alpha = \frac{\alpha^+ + \alpha^-}{2} \tag{16}$$

$$\grave{\alpha} = \frac{\alpha^+ - \alpha^-}{2} \tag{17}$$

where $\alpha^{\pm}$ is described as follows with $D_{\pm}$ being the ion diffusivity.

$$\alpha^{\pm} = \frac{\varphi_T^2 \, \varepsilon_m}{\eta \, D_{\pm}} \tag{18}$$

The k terms from above are defined as follows.

$$k_0 = 80 + (357\alpha - 80\,\dot{\alpha})\zeta_0 + \left(210\alpha - 840\alpha^2 \ln(2)\right)\zeta_0^2 + 210\alpha(\alpha - \dot{\alpha})\,\zeta_0^3 \tag{19}$$

$$k_1 = 1787 + 4(357\alpha - 80\,\dot{\alpha})ln(2) \ldots$$

$$+ \left(42\alpha\left(-160\alpha\,ln^2(2) + 103 + 66\,ln(2)\right) - 1237 - 42\dot{\alpha}\right)\zeta_0 \ldots$$

$$+ (672\alpha(11\alpha + 4\dot{\alpha})\,ln(2) + 1974\alpha + 84\dot{\alpha})\,\zeta_0^2 + 42(\alpha - \dot{\alpha})(49\alpha + \dot{\alpha})\,\zeta_0^3 \tag{20}$$

$$k_2 = 4\left[\left(42\alpha\left(-80\alpha\,ln^2(2) + 103 + 46\,ln(2)\right) - 1237\dot{\alpha}\right)ln(2) + 42\left(83 + ln(4096)\right)\right] \ldots$$

$$+4\left[-21\alpha\left(8(103\alpha + 17\dot{\alpha})ln^2(2) - 191 - 366\,ln(2)\right) - 1669\dot{\alpha} - 315\right]\zeta_0 \ldots$$

$$+4[-21(65\alpha^2 + 152\alpha\dot{\alpha} + 3\dot{\alpha}^2)\,ln(4) + 966\alpha + 189\dot{\alpha}]\zeta_0^2 \ldots$$

$$+252(\alpha - \dot{\alpha})(19\alpha + \dot{\alpha})\zeta_0^3 \tag{21}$$

$$k_3 = 2[-8064\alpha(9\alpha - \dot{\alpha})ln^3 2 + 336(121\alpha - 2\dot{\alpha})\,ln^2 2 \ldots$$

$$+8(4011\alpha - 1669\dot{\alpha} + 987)ln2 + 23786$$

$$+2[84(-4(227\alpha^2 + 160\alpha\dot{\alpha} + 3\dot{\alpha}^2)ln^2 2 + (219\alpha + 2\dot{\alpha})ln4 + 105\alpha) - 7342\dot{\alpha} - 3696]\,\zeta_0$$

$$+504[(\alpha - 3\dot{\alpha})(19\alpha - \dot{\alpha})\,ln4 - 5\alpha + 3\dot{\alpha}]\zeta_0^2 \tag{22}$$

$$k_4 = 16[-168(163\alpha^2 + 56\alpha\dot{\alpha} + \dot{\alpha}^2)ln^3 2 + 84(173\alpha - 7\dot{\alpha})\,ln^2 2 \ldots$$

$+ (4010\alpha - 3671\grave{\alpha} + 1470)ln2 + 4528 \dots$

$+ 48[84(19\alpha - \grave{\alpha})(\alpha - 3\grave{\alpha})ln^2 2 - 84(6\alpha + \grave{\alpha})ln2 + 235\grave{\alpha} + 168] \zeta_0$ \hfill (23)

$k_5 = 192[-84(\alpha - \grave{\alpha})(19\alpha - \grave{\alpha})ln^3 2 - (422(\grave{\alpha} - 17\alpha)ln2 + 235\grave{\alpha})ln2 \dots$

$+209 + 42ln2$ \hfill (24)

By combining the linear and nonlinear EP velocities together, the total particle velocity can be stated as:

$$\vec{v}_p = \vec{v}_{EP}^{(1)} + \vec{v}_{EO} + \vec{v}_{EP}^{(3)} = \mu_{EP}^{(1)} \vec{E} + \mu_{EO}\vec{E} + \mu_{EP}^{(3)} (\vec{E} \cdot \vec{E})\vec{E}$$ \hfill (25)

For the case of an electrokinetically "trapped" particle, the particle velocity will be zero and the following equations hold true [15].

$$E_{EEC} = \sqrt{-\frac{\left(\mu_{EP}^{(1)}+\mu_{EO}\right)}{\mu_{EP}^{(3)}}}$$ \hfill (26)

$$\mu_{EP}^{(3)} = -\frac{\mu_{EP}^{(1)} +\mu_{EO}}{E_{EEC}^2}$$ \hfill (27)

1.2.5 Low frequency cyclical separations

There have been a number of successful studies using dielectrophoresis that employ DC and high frequency AC signals [8] but there are very few studies which explore low frequency cyclical signals inside of electrokinetic devices with insulating structures. A previous study by the Lapizco group [25] employed a DC-biased sine cyclical signal to gradually increase the ratio of the linear EK to nonlinear EK forces. This was achieved by decreasing the amount of time the applied

signal was negative. The Ros group has also employed low frequency iDEP separations [26,27]. However, these studies used a high frequency signal with a DC offset to perform the actual separation before using a DC voltage to shift both particles in the same direction.

1.3 List of contributions

This work has furthered the scope of successful EK separation methods by the demonstration of successful separations in an insulator based nonlinear EK device. The study has also contributed to the understanding of nonlinear EP and methods for determining nonlinear EP mobilities.

This work has been published in the following:

Lentz, Cody J., Samuel Hidalgo-Caballero, and Blanca H. Lapizco-Encinas. "Low Frequency Cyclical Potentials for Fine Tuning Insulator-Based Dielectrophoretic Separations."

This work is also in preparation for publication as:

Cody Justice Lentz, Sofia Antunez Vela, Adriana Coll De Peña, Erin Henslee, and Blanca H. Lapizco-Encinas, (in preparation) "Developing a Methodology for the Determination of the Nonlinear Electrophoretic Mobility of Microparticles."

2.0 Research questions

1. **Is it possible to effectively separate particles based on particle size and charge using low frequency cyclical signals inside of an insulator-based electrokinetic device?**

Separations of particles based on size and based on charge within a nonlinear EK device [28].

2. **What kind of signal is optimal for size-based and charge-based particle separations?**

The most effective signal design found for both size-based and charge-based particle separations was the rectangular signal [28].

3. **What signal properties (frequency, amplitude, etc.) should be used for various particle properties?**

It was found that each signal property needed to be considered together in order to have a successful separation [28].

4. **What is the best way to characterize particles for improving simulation?**

The method found to most accurately determine nonlinear EP mobility was the particle image velocimetry (PIV) at high voltage method.

3.0 Methodology

3.1 Microdevices

For this work three different microfluidic devices used, each for a distinct purpose. All devices were molded from polydimethylsiloxane (PDMS) using molds made using standard soft lithography techniques [29]. Devices were cast and cured before being sealed to a PDMS coated glass wafer in order to maintain a consistent zeta potential on each wall. Each device was 10.16 mm in length, 40 µm deep, and contained one inlet and one outlet.

The first device used in this work, shown in Fig. 3, is called a PIV device, has a consistent width of 0.88 mm, and contains no insulating structures. This was used for PIV for linear EK measurements, PIV high voltage $\mu_{EP}^{(3)}$ measurements, and for preliminary aperiodic separations. The purpose of this device is to create a consistent electric field and EOF for particles to experience.
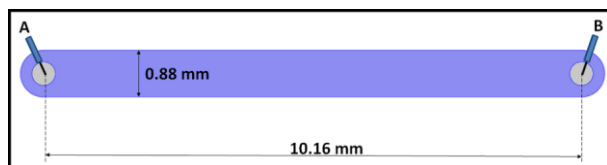
Figure 3: Schematic representation of PIV device with electrodes. Device is 10.16 mm long (as measured from inlet and outlet centers), 0.88 mm wide, and 40 µm deep.

The second device used in this work, shown in Fig. 4, is the circle device, is 0.88 mm wide, and contains cylindrical insulating structures referred to as posts. The posts are 200 µm in diameter, are spaced 20 µm apart in both directions as shown in Fig. 4, and extend though the entire height of the device. The posts are used to constrict the electric field, initially thought of to polarize particles

12

using iDEP (Fig. 2b) but is not known to increase the electric field magnitude and make EP of the second kind considerable.
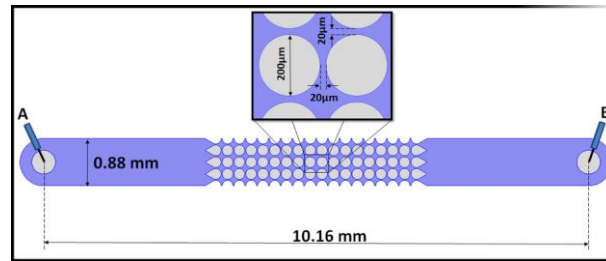
Figure 4: Schematic representation of circle device with electrodes. Device is 10.16 mm long (as measured from inlet and outlet centers), 0.88 mm wide, and 40 µm deep. Post area shown enlarged with post dimensions 20 µm between 200 µm in diameter posts.

The third device used in this study, shown in Fig. 5a, is the funnel device which is based on a design from Weiss et al. [30], is 1 mm wide, and has a gradually constricting center. The funnel shape creates an electric field which linearly increases before linearly decreasing (Fig. 5b). This device was used for the funnel trapping method for determining $\mu_{EP}^{(3)}$ by mapping the location of a trapped particle onto the electric field magnitude.
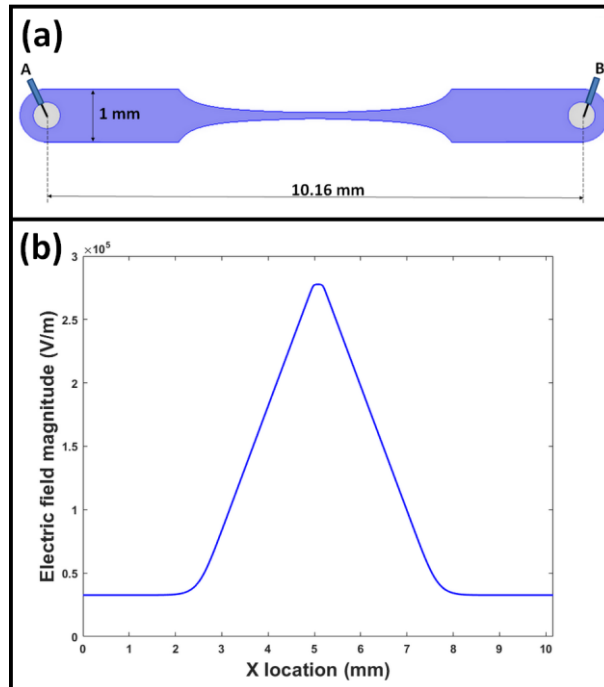
Figure 5: (**a**) Schematic representation of funnel device with electrodes. Device is 10.16 mm long (as measured from inlet and outlet centers), 1 mm wide at its widest, and 40 µm deep. (**b**) Graph of electric field magnitude along the centerline of the device. Electric field is constant in the entrance and exit of device but linearly related to distance for the curved portion of the device.

3.2 Microparticles and suspending media

The particles used in this study were florescent micron-sized polystyrene particles which are useful representations of cells. All particles were suspended in one of two solutions of deionized water with surfactant added to decrease particle aggregation and salt to stabilize pH and conductivity. The suspending media used for the first part of this study used a media with 0.05% (v/v) of Tween 20 with KOH and KCl added to obtain a wall zeta potential (ζ_{wall}) of -93.9 mV in the PDMS devices. This mixture resulted in a pH of 6.0-6.5 and a conductivity of 20-25 µS/cm. The particles in this study using this media are particles 1-4. These particles were selected such that

14

particle 1 and 2 have similar sizes (9.7 vs 10 µm) but differing charges (-19 vs -60 mV) while

particles 2 and 3 had similar charges (-58 vs -48 mv) but differing sizes (2 vs 5.1 µm). All particles

in this first solution had concentrations of $1.8 \times 10^6 - 2.0 \times 10^8$ particles/mL.

TABLE 1: List of particles used in first half of study (particle 1-4) with associated properties. The particle zeta potential, EK mobility, and DEP mobility were found experimentally. Reported uncertainties for $\zeta_{particle}$ and μ_{EK} are one standard deviation. Reported uncertainties for μ_{DEP} are based on the accuracy of the image-based determination of trapping distance and the uncertainty of μ_{EK}.

#	Brand	Color	Diameter (µm)	Surface Funct.	$\zeta_{particle}$ (mV)	μ_{EK} x 10^8 ($m^2V^{-1}s^{-1}$)	μ_{DEP} x 10^{18} ($m^4V^{-2}s^{-1}$)
1	Magsphere	Green	9.7	Carboxylated	-19 ± 11	5.66 ± 0.20	-7.58 ± 0.031
2	Invitrogen	Red	10	Carboxylated	-60 ± 6	2.40 ± 0.30	-2.80 ± 0.40
3	Magsphere	Green	2	Carboxylated	-58 ± 15	2.61 ± 0.26	-1.70 ± 0.19
4	Magsphere	Red	5.1	Carboxylated	-48 ± 5	3.38 ± 0.35	-4.63 ± 0.56

For the second part of this study, deionized water with 0.05% (v/v) of Tween 20 was used

as before, but K_2HPO_4 was added to create a 0.2 mM solution so that the nonlinear EP mobility

could be accurately calculated using the theoretical model. This solution a conductivity of 41

µS/cm and a pH of 7.33. The wall zeta potential (ζ_{wall}) was found to be -72 mV using current

monitoring. Particles 5-8 were suspending in this second media and had concentrations ranging

from 1.5×10^5 to 5.7×10^6 particles/mL.

TABLE 2: List of particles used in second half of study (particle 5-8) with associated properties. The particle zeta potential, EK mobility, and EP of the second kind mobility were found experimentally. Reported uncertainties for $\zeta_{particle}$, μ_{EK}, and $\mu_{EP}^{(3)}$ are one standard deviation.

#	Brand	Color	Diameter (μm)	Surface Funct.	$\zeta_{particle}$ (mV)	μ_{EK} x 10^8 (m²V⁻¹s⁻¹)
5	Invitrogen	Red	2.0	Carboxylated	-58 ± 4	1.06 ± 0.32
6	Magsphere	Red	2.0	Carboxylated	-0 ± 3	5.56 ± 0.22
7	Magsphere	Green	5.1	Non-Funct.	-28 ± 2	3.40 ± 0.19
8	Magsphere	Green	6.8	Carboxylated	-19 ± 2	4.06 ± 0.13

3.3 Equipment and software

Microparticles were observed using a Leica DMi8 inverted microscope (Wetzlar, Germany) with a Leica DFC7000 T camera and the software LASX. Voltages were applied using a high voltage supply (HVS3000D, LabSmith, Livermore, CA). Finite element analysis for electric field modeling was performed using COMSOL Multiphysics 4.4 and FIJI (ImageJ) was used to perform PIV analysis.

3.4 Linear electrokinetic mobility measurements

In order to estimate linear EK velocities and to estimate the particle charge ζ_P it was necessary to find the μ_{EK} for each particle as well as μ_{EO} for the channel. The μ_{EK} for each particle

was found using PIV (Fig. 6a) to obtain particle velocity at three distinct voltages (Fig. 6b)

allowing for the estimation of μ_{EK} using Eqn. 3 [31]. In order to obtain μ_{EO} current monitoring [32]

was performed by filling a long PIV channel with the media of interest before filling the inlet with a

slightly lower conductivity media and applying a voltage. The result is that the device will fill with

a lower conductivity media at the same rate as EOF moves through the device. By analyzing the

current change over time, the velocity of EOF can be found and μ_{EO} can be obtained using Eqn. 2.

Finally, by combining the known μ_{EO} and μ_{EK} mobilities the μ_{EP} can be solved for as well as ζ_P in

Table 1 and 2 by using Eqn. 1.
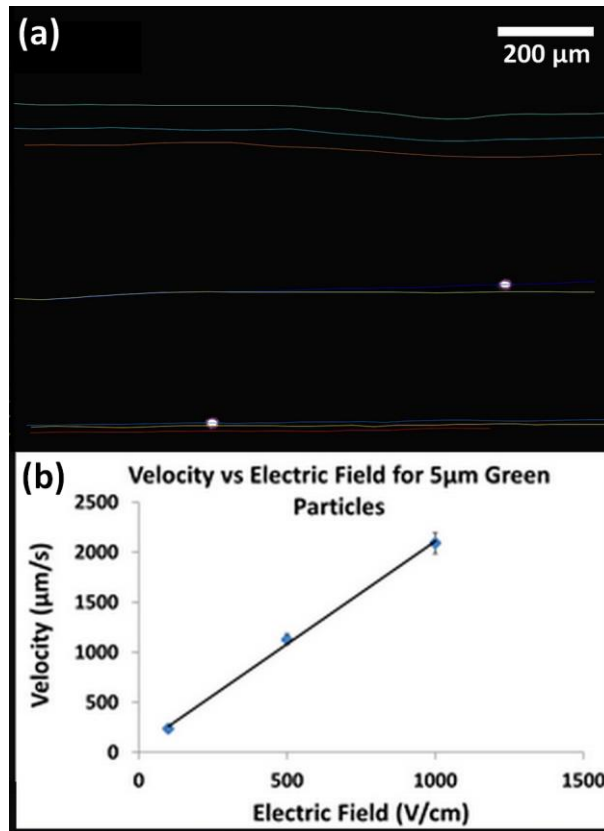
Figure 6: (**a**) Traces of particle tracks using ImageJ. (**b**) Graph of particle velocity vs. electric field. The
slope of this graph is the μ_{EK} of the given particle.

17

3.5 Dielectrophoretic mobility measurements

In order to accurately model the movement of particles assuming linear EK forces and DEP forces are significant, particle μ_{DEP} must be estimated using Eqn. 8. Each particle's μ_{EK} was found as previously discussed but the $|\nabla E^2|$ and $|\vec{E}|$ experienced by the particle when there is zero velocity must be estimated separately. In order to obtain this, particles are introduced into the circular posts channel and a voltage is applied such that a single particle can be seen having zero velocity between insulating posts (see Fig. 7a). The distance between the particle and post centerline was measured (Fig. 7a) and used to find $|\nabla E^2|$ and $|\vec{E}|$ at that distance using a COMSOL model (Fig. 7b). the resulting μ_{DEP} values are reported in Table 1.
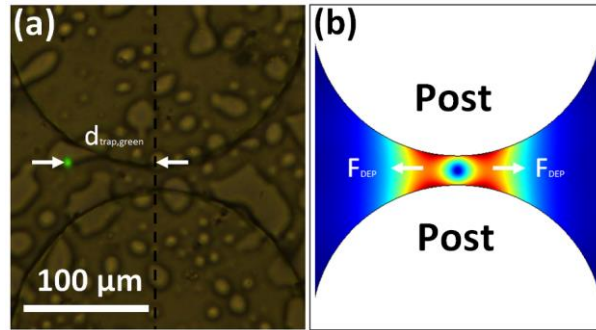
Figure 7: (**a**) Image of trapped particle and posts. Particle trapping distance from centerline (shown as dashed black line) is shown in white. (**b**) Graph of ∇E^2 inside constriction with arrows representing DEP force direction.

3.6 Nonlinear electrophoretic mobility measurements

In order to predict particle migration based on linear EK and nonlinear EP forces (Eqn. 25), the $\mu_{EP}^{(3)}$ of each particle of interest must be estimated. In the second half of this study three different

methods (PIV high voltage (PIV-HV), funnel, and circler posts) were developed in order to estimate $\mu_{EP}^{(3)}$.

3.6.1 Particle image velocimetry at high voltage

The first and simplest method developed was PIV-HV and consists of applying three voltages considerably above the ones used for the PIV measurements for μ_{EK}. Preliminary experiments were run to estimate visually at what voltage the particles stop increasing in velocity. After videos of particles moving at high voltage were captured, videos were analyzed using PIV and the resulting velocities, plotted in Fig. 10, were used to estimate $\mu_{EP}^{(3)}$ using Eqn. 25.
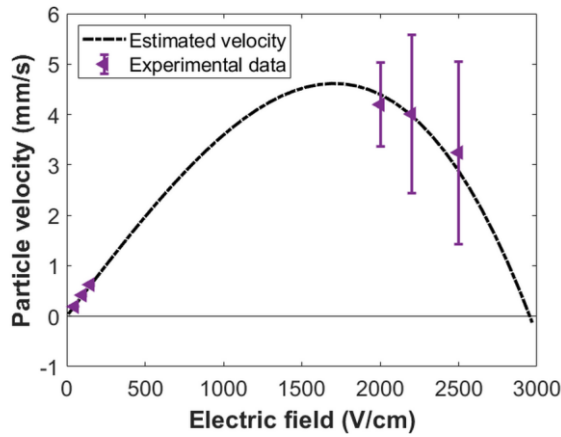
Figure 8: Graph of particle velocity vs. electric field. Both experimental and predicted velocities. Experimental error bars represent one standard deviation.

3.6.2 Funnel trapping

The second method for estimating $\mu_{EP}^{(3)}$ was funnel trapping and uses the fact that according to Equation 25 particles will trap at a certain electric field magnitude known as the particle's E_{EEC}. Once a particle's E_{EEC} is known the $\mu_{EP}^{(3)}$ can be calculated using Equation 27. The device used is a

funnel device with a linearly increasing electric field (Fig. 5) in order to avoid rapid special changes in electric field which would cause the uncertainty in particle location to cause large uncertainties in $\mu_{EP}^{(3)}$. Particles were trapped in the first half of the constriction (Fig 8a/b) and images were obtained of the trapped particles (Fig 8b). These images were then post processed using a custom Matlab program to obtain E_{EEC} and $\mu_{EP}^{(3)}$ values.
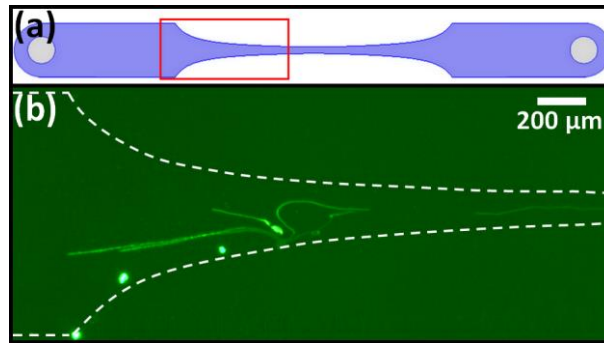
Figure 9: (**a**) Schematic representation of funnel device with viewing area shown in red. (**b**) Image of particles trapping in entrance to funnel device.

3.6.3 Circular post trapping

The third method of $\mu_{EP}^{(3)}$ estimation is circular post trapping and also relies on determination of E_{EEC} to then find $\mu_{EP}^{(3)}$. Various voltages were tested to determine a voltage where particles trap between post in the same way as the μ_{DEP} estimation method. Images of trapped particles were taken (Fig. 9a) and post processed using a custom Matlab script. The script uses subpixel localization [33] to obtain a and curve-fitting of the outline of posts the particle location with an uncertainty which is less than a pixel width. Particle location data was then used to estimate particle E_{EEC} by linearly interpolating electric field data from COMSOL simulations (Fig. 9b).
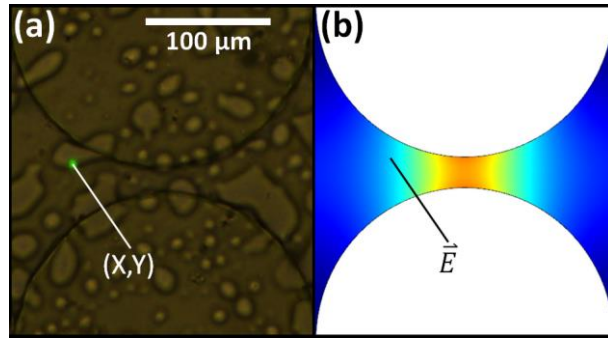
Figure 10: (**a**) Image of particle trapped in post constriction. (**b**) Graph of electric field in constriction.

4.0 Results

The results from this work are separated into two parts: the first was particle separations assuming linear EK and DEP forces and the second was developing a methodology for estimating $\mu_{EP}^{(3)}$ which can later be used for separation design. Before particle separation could take place using low frequency cyclical signals a separation method was devised (Fig. 11) as well as a custom Matlab script for simulating particle migration for low frequency cyclical signals (Fig. 12-13). Particles were successfully separated based on charge (Fig. 14-15) and by charge (Fig. 16) using low frequency cyclical signals after simulating a variety of signals to achieve a signal which worked according to simulation. For the second part of this work, three different methodologies for estimating $\mu_{EP}^{(3)}$ were tested (Fig. 18) and the best method was tested on four particle species (Fig. 19). These four $\mu_{EP}^{(3)}$ were then compared to the mobilities predicted by the theoretical model (Table 3).

4.1 Method for cyclical separation

After some preliminary testing, the method behind low frequency cyclical separation was found to be a three-step process shown in Figure 11. Step 1 is where both particles are trapped on the left side of the constriction (Fig. 11b-c) which is achieved by applying a high voltage (V_H Fig 11a). Then, after a stable trapping is achieved, during step 2 a low voltage (V_L) is applied (Fig. 11a) allowing both particles to move forwards (Fig. 11b-c). The length for which V_L is applied (P_L) combined with the magnitude of V_L must be specially tuned such that at the end of step 2 the slow particle (green in Fig. 11b-c) will be on the left of the constriction and the fast moving particle (red in Fig. 11b-c) is to the right side. For step 3 V_H is applied again and the DEP force will force the

slow-moving particle back to the original trapped position while the fast-moving particle will proceed to be trapped at the next constriction.
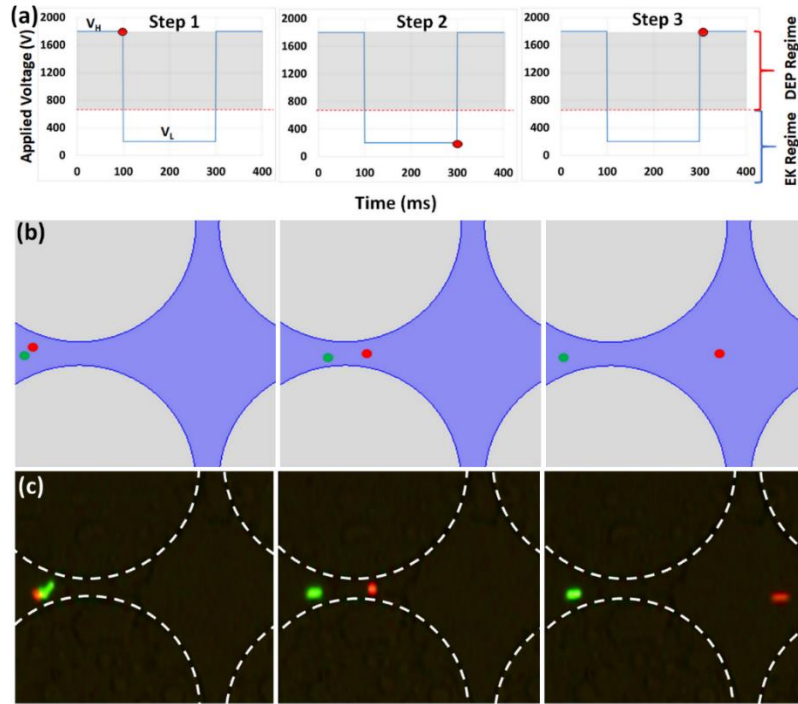
Figure 11: (**a**) Graph of applied voltage vs. time with the voltage at each step indicated in red. Grey part of graph labeled at DEP regime, where particles will trap in the constriction. Lower part of graph in white indicates EK regime where particles are able to stream through the constriction. (**b**) Cartoon representation of the three steps of the separation process where the green dot represents the slow moving particle and red representing the fast moving particle. (**c**) Images of the three steps of particle separation with the green particle being the slow moving particle and the red particle being the fast moving particle.

When tuning the signal to obtain a successful separation there are three failure modes: no particle trapping, no particle migration, or both particle migration. The issue of no particle trapping is rarely an issue because the trapping voltage is known from determining μ_{DEP} and P_H was kept at 100 ms so that the trapping behavior could be recorded using the microscope. When no trapping

was observed V_H was simply increased till this was failure was not observed. The second failure mode, no particle migration, is caused by the fast-moving particle not going far enough though the constriction at the end of step 2. This can be solved by decreasing V_H thereby causing the particles to trap closer to the post centerline and decreasing the distance that step 2 needs to cover. The other and more useful solution is to cause step 2 to cover a further distance by increasing V_L or P_L. The third failure mode, both particle migration, can be solved by the exact reverse of no particle migration (increasing V_H, decreasing V_L, or decreasing P_L).

4.2 Separation prediction software

The search space of possible cyclical signals is vast because the parameters that can be altered are amplitude, frequency, DC bias, and duty cycle bias. This creates a four-dimensional search space with none of the parameters being able to be solved for in terms of the others. In order to avoid spending an unreasonable amount of time preforming parameter sweeps of experiments, a particle migration simulation software was developed which took an applied signal and particle properties (μ_{EK} and μ_{DEP}) as inputs and produced a plot of particle position over time (Fig. 12). The program used the Euler method of integration on Equation 7 to determine the particle position over time. In order to obtain ∇E^2 and E a COMSOL simulation of the device was preformed and the ∇E^2 and E data was curve fitted using a tenth order polynomial for position and a second order polynomial for applied voltage.
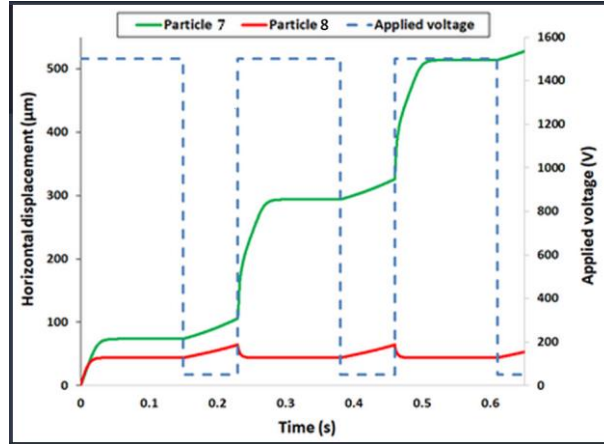
Figure 12: Graph of predicted displacement of 7 (2 µm, green) shown in green and particle 8 (5 µm, red) shown in red when a custom signal, shown in blue is applied.

In order to test the accuracy of the simulation, one particle was placed inside of the device and a cyclical signal was applied and the resulting particle position were tracked using ImageJ. The same particle and signal were simulated and the results were compared showing that the simulation is fairly accurate (Fig. 13). While the real and simulated particle positions are similar, the first and third trapping locations are off. There are a variety of effects which could contribute to modeling inaccuracy including particle movement off of centerline, the true backwards effect being nonlinear EP instead of DEP, particle-particle interactions, Joule heating, and electrothermal flows [22,34,35]. However, none of these effects would systematically change the trapping location for all particles trapped as can be seen in cycles 1 and 3 in Figure 13. The discrepancies in trapping position are more likely caused by inconsistencies within the device, meaning the first constriction was wider causing a lower electric field and the width of the third constriction was smaller causing a higher electric field. While it may seem odd that the simulation is this accurate while assuming the wrong phenomena, DEP instead of EP of the second kind, this can be explained by further consideration. In the case of particle trapping, V_L was always kept close to the voltage used when

25

determining μ_{DEP}, this fact would result in the trapping location being accurate during this test but not if a different device or much different voltage was used. In the case of particle streaming, V_L was kept low for all experiments so that DEP forces would be low. This choice caused the side effect of making EP of the second kind forces low as well meaning that the simulation predicted mainly linear EK forces which as accurate. The only case where the simulation would be substantially inaccurate then is in the start of step 3 (Fig. 11). This discrepancy cannot be seen in Figure 13 as the event is too fast to be seen using our camera. However, the discrepancy in the start of step 3 (Fig. 11) does account for the difference in the simulated working separation and the true separation seen in the separation by charge and separation by size experiments discussed later.
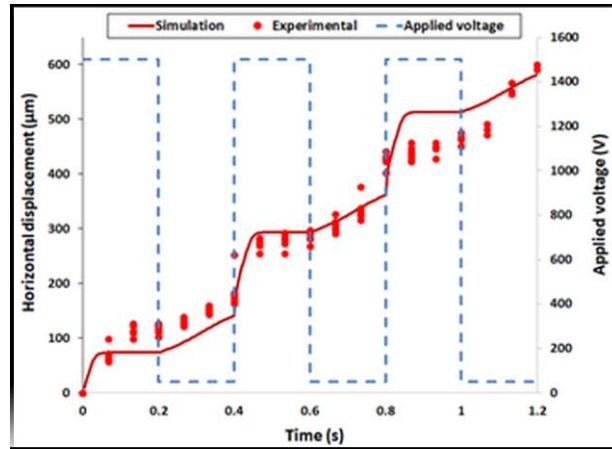
Figure 13: Graph of predicted particle position of particle 8 represented with a red line, experimentally found particle positions of particle 8 represented by red dots, and applied voltage represented by blue dashed line.

4.3 Particle separation by charge

The first demonstration of this method for separation was separation by size where particles were distinguished by differences in linear EK velocity (Eqn. 7). The particles separated, particles 1

(green) and 2 (Red) (Table 1), were both 10 µm in diameter but differed in ζ_P (19 mv vs. 60 mv). Because of the difference in μ_{EK} particle 1 will trap closer to the post centerline than particle 2 during step 1. During step 2, particle 1 will also move faster than particle 2. This particle mixture was separated using two different signal shapes, rectangular (Fig. 14) and sawtooth left (Fig. 15) both of which achieved a successful separation.

The separation by charge using a rectangular signal used a V_H of 1000 V (Fig. 14a) in order to trap both particles (Fig. 14b), a P_H of 0.2 s, a V_L of 200 V (Fig. 14a) in order to allow both particles to stream (Fig. 14c), and a P_L of 0.1 s. Particle 1 (green) migrated an average of 387 µm/s while particle 2 (red) remained in the same constriction and averaged a migration speed of 6.2 µm/s (Fig. 14a). The migration of particle 2 was effectively zero. However, because the particle tracking was started from a frame where the particles were trapped, all proceeding particle positions in frames were positive causing the net migration to be non-zero. In order to find the signal for this separation, many different rectangular signals using the custom Matlab program to find a signal which worked well. Then the signal from simulation was tested and adjustments were made to obtain a working signal. The same adjustments were made to the signal in both simulation and experimentation as was described in Section 4.1.

Figure 14: (**a**) Plot of tracked particle positions, particle 5 and particle 6. Applied rectangular signal plotted in dashed blue line. (**b**) Image of both particles trapped at 1000 V part of signal. (**c**) Image of particle 5 in the entrance to the constriction and particle 6 in the exit of the constriction resulting in particle separation.

While the methodology of separation discussed previously (Fig. 11) used a rectangular signal, a similar methodology can be used with other signal shapes. A variety of signals were tested (rectangular, sine, triangular, sawtooth left, sawtooth right) in simulation and experimentally with two signal shapes working repeatably, rectangular (Fig. 14) and sawtooth left (Fig. 15). The sawtooth left signal starts at a high voltage before linearly decreasing and then immediately returning to the high voltage (Fig. 15a). Both particles will trap at the start of the signal because the voltage is high (Fig. 15b) and stream later in the signal when the voltage is low (Fig. 15c). Because the signal smoothly decreases there is also a point at which the faster moving particle (particle 1 in

28

this case) The sawtooth left signal used to separate particle 1 from particle 2 had an amplitude of

1800 V, a DC offset of 900 V to keep the signal positive, and a period of 0.3 s (Fig. 15a). The

resulting separation showed particle 1 migrating an average of 530 µm/s while particle 2 migrated

an average of 1.5 µm/s without moving to the next constriction.

Figure 15: (**a**) Plot of tracked particle positions, particle 5 and particle 6. Applied sawtooth left signal plotted

in dashed blue line. (**b**) Image of both particles trapped at high voltage part of signal. (**c**) Image of particle 5

in the entrance to the constriction and particle 6 in the exit of the constriction resulting in particle separation.

4.4 Particle separation by size

Based on Equation 4, particle μ_{DEP} is related to the size of the particle squared so a

difference in particle velocity would occur if particles had different sizes even if the particle

charges were the same. This difference in velocity can be exploited using the methodology previously discussed by having the larger particle be the slower moving particle. The larger particle will trap at a further distance from the post centerline but, unlike in separation by charge, the movement of the particles through the constriction at V_L will be similar because the linear EK velocity is the same and nonlinear EK forces are less significant at the lower voltage. It is now known that, due to EP of the second kind, the larger particle will experience a trapping at a further distance because a lower magnitude electric field (E_{EEC}) will be needed to trap the particle (Eqn. 26) caused by $\mu_{EP}^{(3)}$ being related to the size of the particle squared.

The development of a signal for separation by size followed the same process as was used as for the separation by charge; particle properties were obtained and a variety of signals were simulated before experimentally testing signals which worked in simulation and altering to obtain a working signal. The signal (Fig 16a) used a V_H of 1500 V to trap both particles (Fig 16b) with particle 3 (2 µm green) further into the constriction than particle 4 (5.1 µm red) because EP of the second kind is a greater negative force on the larger particle. P_H was set to 0.15 s in order to achieve a stable trapping position. V_L was let to 50 V so that linear EK would dominate nonlinear effects for the 0.08 s (P_L) it was applied. The resulting separation had particle 3 moving at 320 µm/s on average while particle 4 migrated 1.5 µm/s on average. Unlike with separation by charge, there is a higher distribution of migration speed as can be seen in Figure 16a. This is caused by the fact that instead of the particles separating during the application of V_L the particle 4 migrated closer to particle 3 because particle 4 has a zeta potential lower than that of particle 3 (48 mv vs. 58 mv) causing the linear EK velocity of particle 4 to be higher than particle 3.
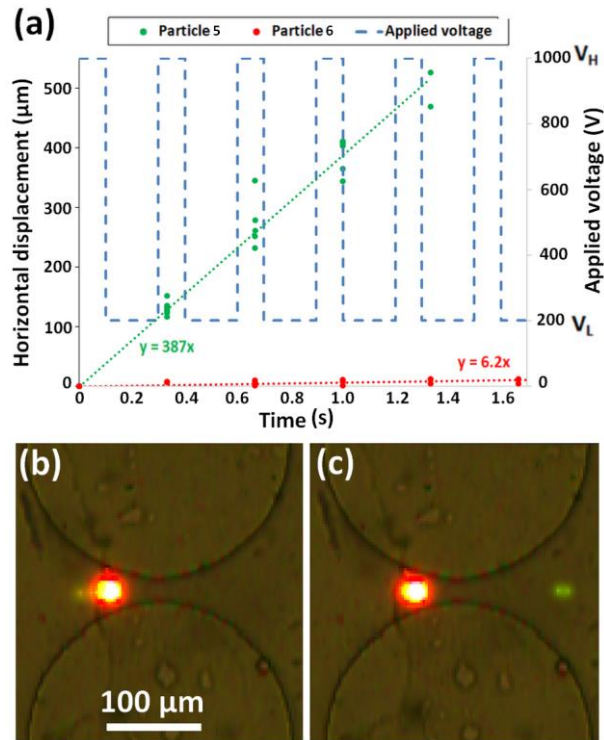
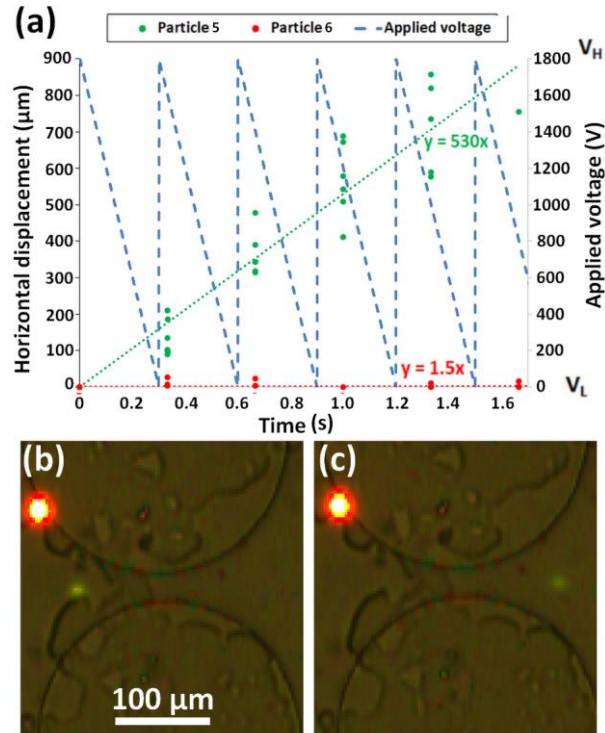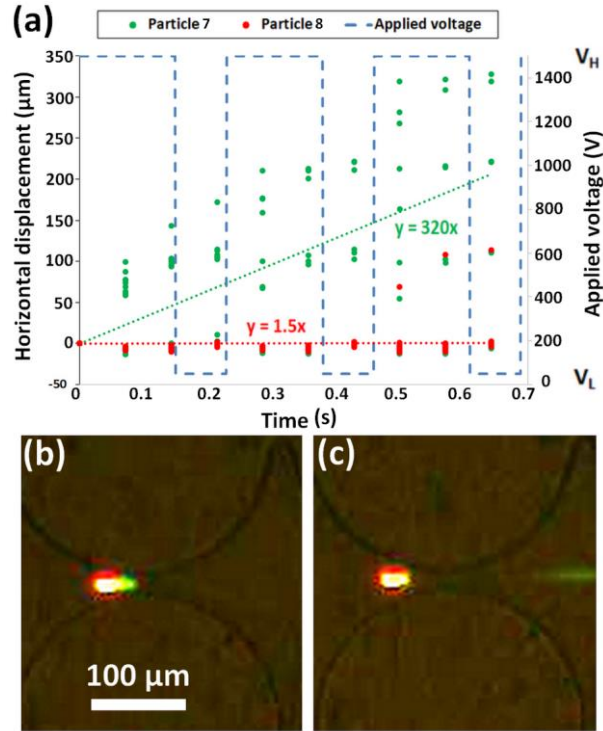**Figure 16:** (**a**) Plot of tracked particle positions, particle 7 and particle 8. Applied rectangular signal plotted in dashed blue line. (**b**) Image of both particles trapped at 1500 V part of signal. (**c**) Image of particle 7 in the entrance to the constriction and particle 8 in the exit of the constriction resulting in particle separation.

4.5 Comparison of dielectrophoresis to nonlinear electrophoresis

The first part of this study, which has been discussed in the previous four sections, assumed the dominate nonlinear EK force inside our systems was DEP but this assumption is now under scrutiny. Studies of DEP which employ AC signals have been modeled with good accuracy [8], however, DEP systems which employ DC signals have had discrepancies between the theoretical and observed DEP force magnitudes [34]. These discrepancies were as much as a factor of 600, indicating that there are clearly inaccuracies with the model. Issues also have arisen with the particle behavior observed in our devices. According to linear EK and DEP, trapped particles

31

should be trapped when the linear EK and DEP vectors oppose each other and the angle between the vectors would be zero (Fig. 17a). These vectors are not opposing each other for all of the constriction area, in fact, only a narrow band and the area around the horizontal centerline would offer places where particles could theoretically trap (Fig. 17b). When comparing the possible trapping areas (Fig. 17b) to the observed area of trapped particles (Fig. 17c /15b) it is clear that there is a significant force other than DEP and linear EK responsible for particle trapping.
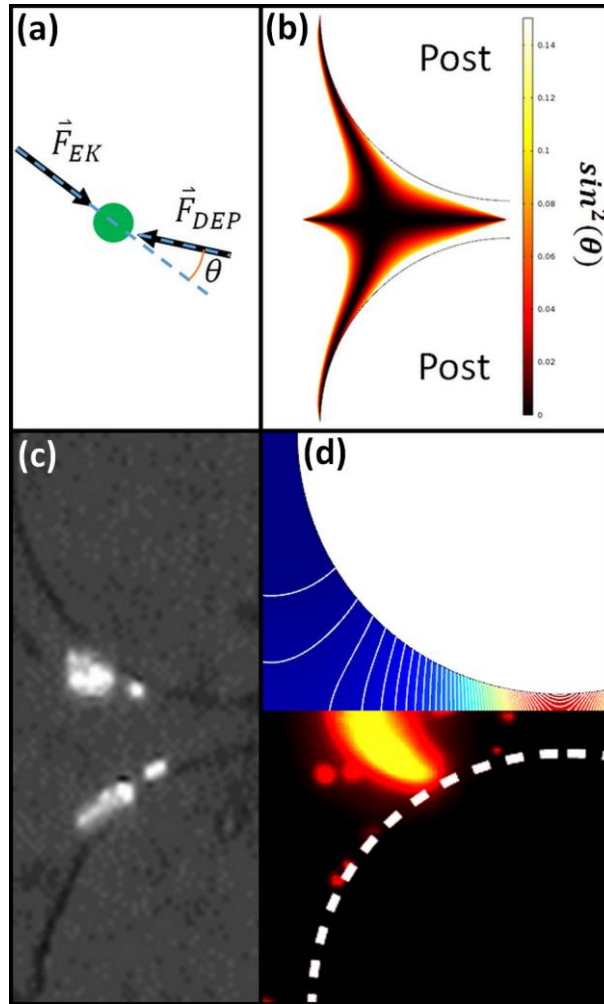
Figure 17: (**a**) Diagram of linear EK and DEP forces present on a particle trapping under that theory. Angle between the forces is shown by θ. (**b**) Plot of the $\sin^2(\theta)$ where θ is the angle between linear EK and DEP forces inside constriction. Dark areas indicate where the $\sin^2(\theta)$ is low and particles would trap due to DEP. (**c**) Image of trapped particles in constriction which are notably outside of the dark area in part b. (**d**) Plot of electric field with white isoelectric lines compared to image of a band of trapped particles.

A study currently in preparation by the Perez-Gonzalez group [15] suggests that DEP forces in most DC iDEP systems are negligible and that the main forces present are linear EK and nonlinear electrophoresis [1,12,15,23]. If EP of the second kind is the main force causing particle

trapping would mean particles should trap along electric field iso-lines, which as can be seen in

Figure 17d appears to be true, and would not have the same issue of force angles (Fig. 17a-b). Even

if nonlinear EP forces are the dominant force, DEP forces could still be present as the electric field

gradient is still present. This concern was addressed in a recent study which concluded that for

bacteria and yeast trapping inside of a circle device the contribution of DEP force was under 6% of

that of nonlinear EP and was less than the uncertainty in the measurement of EP force [14]. In light

of these discoveries, this study moved to incorporate nonlinear EP into particle migration

simulation.

4.6 Nonlinear electrophoretic mobility measurements

Before a simulation of a low frequency cyclical separation assuming linear EK and

nonlinear EP forces could be created, the $\mu_{EP}^{(3)}$ of each particle of interest had to be estimated.

Initially, the same method used to predict μ_{DEP} (Section 3.5) was used, however, because nonlinear

EP is dependent on the electric field cubed, the uncertainty in particle position propagated and

caused the $\mu_{EP}^{(3)}$ to have such a large uncertainty as to be non-useful. In light of this, three methods

were developed for determining particle $\mu_{EP}^{(3)}$: PIV HV, funnel, and circular posts. Each of these

methods is described in detail in Section 3.6.

In order to compare these three methods, the $\mu_{EP}^{(3)}$ and associated uncertain of particle 8 was

determined with each. The results, shown in Figure 18, were that the circular posts method was by

far the least accurate and PIV HV being somewhat more accurate than the funnel method. The

circular posts method was least accurate as small differences in the creation of the device geometry

create small differences in particle trapping position which result in high $\mu_{EP}^{(3)}$ uncertainty as the

electric field changes dramatically in the constriction. The results from the funnel method are lower in magnitude than those from PIV HV which is unexpected as DEP forces should be present in the funnel constriction but not in a PIV device. This discrepancy could be attributed to unaccounted for forces such as electrothermal flows which would also explain the erratic particle behavior seen in funnel experiments (see Fig. 8b). Because of the lower uncertainty and the erratic behavior seen in the funnel, PIV HV was selected as the method to create a library of $\mu_{EP}^{(3)}$ data.
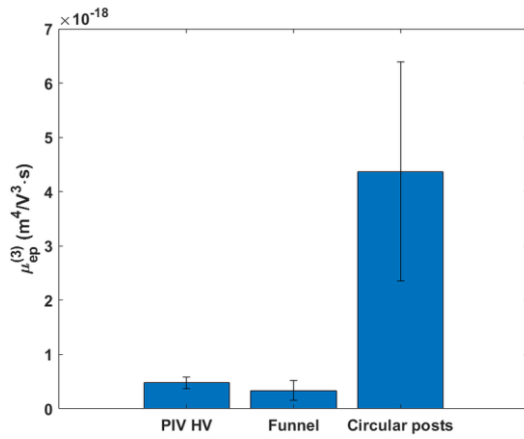
Figure 18: Plot of $\mu_{EP}^{(3)}$ values for particle 8 with three different methods with standard deviations represented by error bars.

The process of PIV HV was repeated as described in Section 3.6.1 for four distinct particle types and the resulting $\mu_{EP}^{(3)}$ values were compiled (Fig. 19). Particle 4 and 5 are 2 µm particle with ζ_P values of ~-58 and ~0 respectively. Contrary to what was initially thought, particle 5 had a higher $\mu_{EP}^{(3)}$ even with a lower charge. Also of note, particles 7 and 8 have by far the lowest $\mu_{EP}^{(3)}$ magnitude and uncertainty. The decreased uncertainty is most likely due to the fact that these particles are larger and therefore can be more easily tracked using PIV.
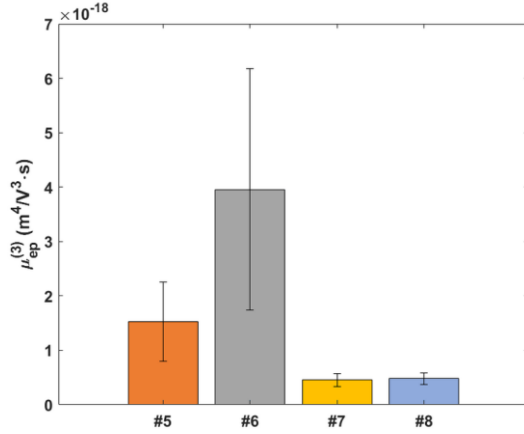
Figure 19: Plot of $\mu_{EP}^{(3)}$ values for particles 5 - 8 with standard deviations represented by error bars.

Once the μ_{EK} and $\mu_{EP}^{(3)}$ were known, Equation 7 could be used to predict particle velocity for all electric field values (Fig. 20). This particle velocity information is useful when simulating particle migration as was performed in Section 4.2 or in separating particle based on differences in E_{EEC} values as has been demonstrated before the understanding of EP of the second kind [13]. In order to use the low frequency cyclical method, the particles to be separated must have sufficient differences in either their E_{EEC}, in order to allow for differences in trapping distances (step 1), or in their linear EK mobility, to allow for differences in migration at low electric fields (step 2). Separation by differences in E_{EEC} are preformed by creating an electric field, commonly inside a constriction, between the E_{EEC} values of the two particle such that only the particle with the higher E_{EEC} could make progress. For example, particle 6 could be trapped while particle 8 would continue migrating if an electric field 2.5x10⁵ V/m created a "barrier" across the device or constriction.
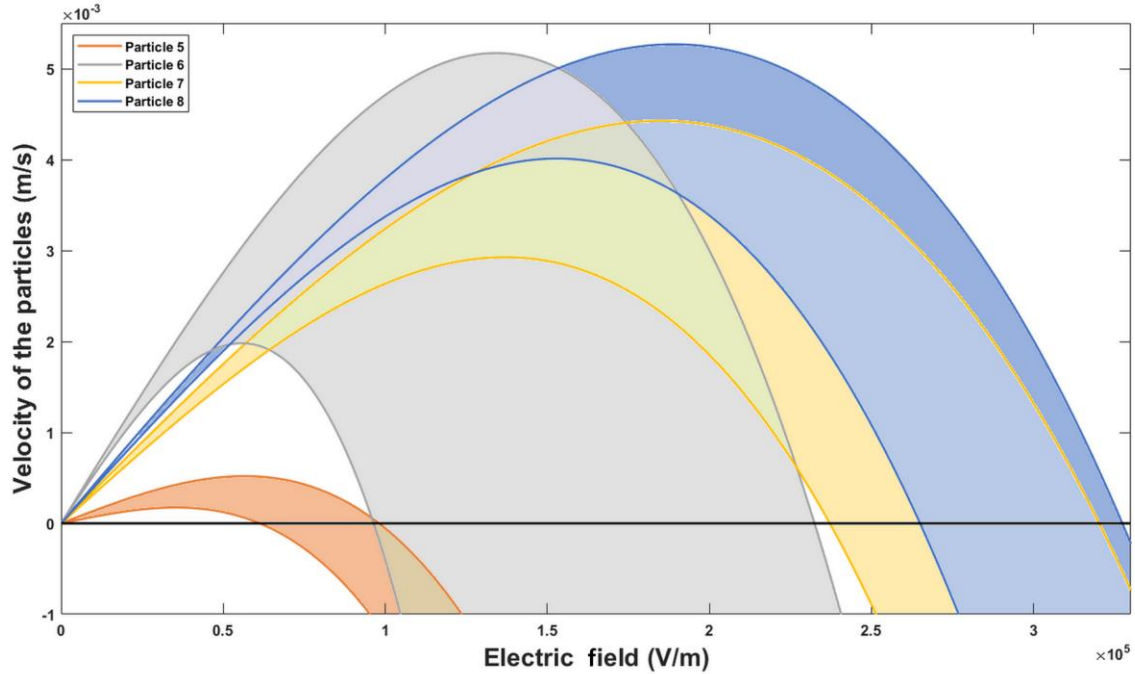
Figure 20: Graph of particle velocity vs. electric field for particles 5 – 8. Width of band indicates one standard deviation of predicted particle velocities.

4.7 Comparison to of experimental and predicted mobilities

Having obtained the values of $\mu_{EP}^{(3)}$ for four different particles and knowing particle and corresponding media properties, it was possible to compare experimental $\mu_{EP}^{(3)}$ with estimates from the dimensionalized version of the model developed by Schnitzer et al., [1] (Eqn. 9). The resulting mobilities, as can be seen in Table 3, have overlapping ranges for particles 6 and 8 but particles 5 and 7 predicted mobilities were 2– 5 times greater than that of experimental mobilities. The upper and lower bounds in predicted $\mu_{EP}^{(3)}$ come from the particle zeta potential input being set to one standard deviation above or below the average value (Table 2-3). The suspending media used for these measurements resulted in a Debye length (λ) of 78 nm, α^+ of 0.2537, α^- of 0.7206, α of

0.4872, and $\dot{\alpha}$ of -0.2335. Because of this the predicted $\mu_{EP}^{(3)}$ could be increased by more accurate

ζ_p, however, for any type of particle there is a population distribution in both ζ_p and consequently

$\mu_{EP}^{(3)}$ as can be seen by the vary particle velocities observed in experiments. The reason for the gap

between predicted and experimental $\mu_{EP}^{(3)}$ for particles 5 and 7 could be a range of inputs (T, η, ε_m,

$D_{\pm}$, λ) caused by joule heating or salt surfactant interactions unaccounted for in the model. It is also

possible that PIV HV causes some systematic error which underestimates $\mu_{EP}^{(3)}$, but this is unlikely

considering the good agreement between PIV HV and the funnel method (Fig. 18).

Table 3: List of value range for predicted and experimental values of $\mu_{EP}^{(3)}$ for particle 5 – 8. Also listed are particle diameter as reported by manufacturer, particle zeta potential as measured experimental, Bi Du, and ζ_0. Error reported as one standard deviation.

#	r_p (μm)	ζ_p (mV)	Experimental $\mu_{EP}^{(3)}$ x 10^{18} ($m^4V^{-3}s^{-1}$)	Bi (-)	Du (-)	ζ_0 (-)	Predicted $\mu_{EP}^{(3)}$ x 10^{18} ($m^4V^{-3}s^{-1}$)
5	2.0	-58 ± 4	-2.25 to -0.80	0.166 to 0.191	-0.405 to -0.465	1.7967 to 1.5204	-5.389 to -4.442
6	2.0	-0 ± 3	-6.17 to -1.74	0.000 to 0.009	-0.0225 to 0.0225	-4.2603 to 4.2603	-4.828 to 4.828
7	5.1	-28 ± 2	-0.57 to -0.34	0.031 to 0.036	-0.0756 to -0.0882	0.3448 to -0.0586	-3.804 to -2.523
8	6.8	-19 ± 2	-0.59 to -0.37	0.015 to 0.019	-0.0375 to -0.0463	-0.7911 to -0.3685	-1.034 to 0.916

The model for $\mu_{EP}^{(3)}$ explains some unusual observations from the experimental results.

Particle 5 and 6 are both 2 µm in diameter, particle 5 is highly charged particle 6 has nearly no

charge, however, the experimental $\mu_{EP}^{(3)}$ of particle 6 is higher than particle 5. This fact indicates that

it cannot be assumed that a larger zeta potential will result in a higher $\mu_{EP}^{(3)}$. According to the model,

the $\mu_{EP}^{(3)}$ of a particle will increase close to linearly with ζ_p only if the ζ_p is above the φ_T (Fig. 21).

When the ζ_p drops below φ_T, the relationship becomes nonlinear and the $\mu_{EP}^{(3)}$ and $\mu_{EP}^{(1)}$ of a particle

can have opposite signs (Fig. 21). This would explain the $\mu_{EP}^{(3)}$ of particle 6 if the ζ_p of particle 6 is

actually positive which is within the uncertainty (Table 2-3). This effect would also explain the

high uncertainty in $\mu_{EP}^{(3)}$ for particle 6 (Fig. 19) when compared to the other particles which have
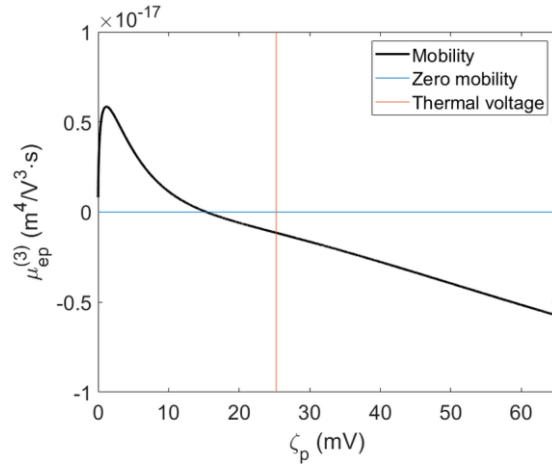
higher charge magnitudes.

Figure 21: Plot of $\mu_{EP}^{(3)}$ for a 2 μm particle suspended in the same media as particles 5 − 8.

5.0 Conclusions

5.1 Summary

The study presented here achieved two main components: separation of particles using a low frequency signal with assistance from a custom simulation [28] and development of a new methodology for the determination of $\mu_{EP}^{(3)}$. The first part of this study assumed linear EK forces and DEP to create the simulation software. The second half started after it was discovered that DEP is much less significant than EP of the second kind. The high uncertainty in the simulation of particle migration after EP of the second kind was used necessitated the development of a new, more accurate, method for determining $\mu_{EP}^{(3)}$, which was undertaken in the second part of this study.

The separation of particles using low frequency cyclical signals was theorized to be capable of separating particles based on charge (exploiting differences in μ_{EK}) or based on size (thought to be exploiting differences in μ_{DEP} but now known to be exploiting differences in $\mu_{EP}^{(3)}$). The basic methodology for separation in this manner is to trap both particles at the extract to a constriction with a high voltage, then apply a lower voltage to allow the fast particle to move through before applying the high voltage again, trapping the fast particle in the next constriction. The signal amplitude, frequency, DC bias, and duty cycle bias necessary to achieve this effect for a pair of particles is nonobvious and experimental tests are too time consuming to make an experimental parameter sweep practical. In light of this, a custom simulation of particle migration inside the device was created. This simulation relied on μ_{EK} values, which was readily available, as well as, μ_{DEP} values, which required the development of a new method, to predict particle migration. Once particle properties were estimated, the particle separation was tested utilizing a variety of signals till

40

a working signal was obtained. Having a signal which was effective in simulation, experiments were run to test for separation and the signal was adjusted to such that effective separation was achieved. This process resulted in the successful separation of two 10 µm particles by exploiting differences in charge of 19 vs. 60 mV in addition to the separation of a 2 µm particle from that of a 5.1 µm particle of approximately the same charge (~50 mV).

After the completion of these separations, it came to the group's attention that the more likely nonlinear EK phenomenon present in the system was EP of the second kind, as opposed to DEP. This change is assumed physics required the development of a new method for determining $\mu_{EP}^{(3)}$. The initial solution to this problem was a modified version of the method for μ_{DEP} estimation. However, because EP of the second kind relies on the electric field cubed instead of the gradient of the electric field squared, the uncertainty in $\mu_{EP}^{(3)}$ was so large as to have no statistical significance between particles of interest. The uncertainty was slightly larger than that reported for circular posts (Fig. 18). Three new methods for $\mu_{EP}^{(3)}$ estimation (PIV HV, funnel, circular posts) were developed and tested on a single particle so that the uncertainty of each could be compared. The PIV HV method was found to be most accurate and was used to develop a library of four particle with associated ζ_P and $\mu_{EP}^{(3)}$. These results were compared to $\mu_{EP}^{(3)}$ values estimated from the model (Eqn. 9).

5.2 List of contributions

This work has displayed the following:

1. Separation of particles by size using low frequency cyclical signal in nonlinear EP device.

2. Separation of particles by charge using low frequency cyclical signal in nonlinear EP device.

3. Simulation of particle position over time in a nonlinear EP device for time dependent signal.

4. Development of three different methodologies for estimation of nonlinear EP mobility.

5. Comparison of methodologies for estimation nonlinear EP mobility.

6. Comparison of experimental and theoretical estimations of nonlinear EP mobility.

This work has been published in the following:

Lentz, Cody J., Samuel Hidalgo-Caballero, and Blanca H. Lapizco-Encinas. "Low Frequency Cyclical Potentials for Fine Tuning Insulator-Based Dielectrophoretic Separations."

This work is also in preparation for publication as:

Cody Justice Lentz, Sofia Antunez Vela, Adriana Coll De Peña, Erin Henslee, and Blanca H. Lapizco-Encinas, (in preparation) "Developing a Methodology for the Determination of the Nonlinear Electrophoretic Mobility of Microparticles."

5.3 Future work

While a methodology for determining $\mu_{EP}^{(3)}$ was developed in this study, there exists a need for a more accurate method in order to build a library of bioparticle mobilities which could be used in lab on a chip applications. The E_{EEC} ranges Figure 20 are far wider than previous experiments, which assumed iDEP [36], would suggest. The uncertainty in particle mobility is of great importance for separation, as it allows for the prediction of what can be separated and using what

voltage/method. The useful uncertainty in $\mu_{EP}^{(3)}$ is the population distribution, differences in true $\mu_{EP}^{(3)}$ between particle, and therefore using a large number of measurements to decrease uncertainty is not optimal. Because of this, it would be useful to develop a more accurate method such as aperiodic EP (APEP) as described below.

Having a more accurate measurement of $\mu_{EP}^{(3)}$ coupled with the more accurate understanding of physical phenomena occurring within the device should allow for more accurate simulation and therefore better separations of particle using low frequency cyclical signals. While this may be the case, inconsistencies in device manufacturing would still cause issues in trapping distances and particle migration estimations. Because of the understanding of EP of the second kind, it is possible to separate particles by size using a PIV device (Fig. 3) which has no posts by using APEP as discussed later. While using a PIV style device avoids large effects from manufacturing differences, using low frequency cyclical signals creates issues when using EOF. In the steady state case, EOF creates a very flat velocity profile (Fig. 1a) because the force causing fluid motion is the EP migration of ions near the walls of the device but the fluid movement must propagate from the walls to the center of the device. This process can take on the order of 10 ms [37] and, because the velocity propagates from the walls, this delay in drag from EOF changes with a particle's vertical location in the device as well as the particle's location in the horizontal plane if it is near a constriction. Because of this, APEP would be more accurate if low frequency was avoided and frequencies above ~1 kHz were used.

5.3.1 Aperiodic electrophoresis for mobility measurements

The bases for APEP was developed by Dukhin and Dukhin [38] to exploit $\mu_{EP}^{(3)}$ by applying a signal which had a time averaged electric field of zero but a time averaged electric field cubed

43

which was nonzero. This kind of signal is shown using a combination of sine signals in Fig. 22a and using a rectangular signal in Fig. 22b. This type of signal causes the linear EK migration to be zero over one period but the nonlinear EP migration to be nonzero. The resulting particle velocity could be found using PIV and $\mu_{EP}^{(3)}$ could be calculated after averaging the particle velocity (Eqn. 9) over the signal period. Using a frequency above 1 kHz would negate EOF effects, because the fluid migration would not have time to propagate in addition to minimizing joule heating and electrothermal flows [38].
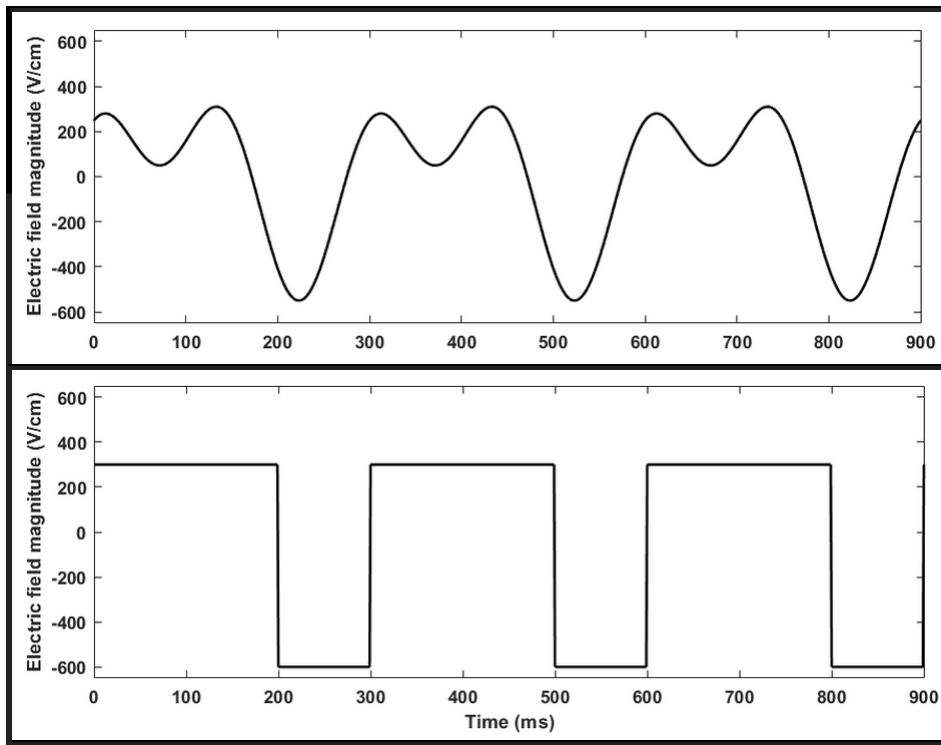

Figure 22: Plot of example aperiodic signals with net zero electric field but nonzero electric field cubed. (**a**) Plot of combined sine signal with one sine with a 300 V amplitude and the other with a 250 V amplitude and twice the frequency. (**b**) Plot of rectangular signal with 300 V being applied for 200 ms before applying -600 V for 100 ms.

5.3.2 Aperiodic electrophoresis for particle separations

Not only does APEP have the ability to provide particle $\mu_{EP}^{(3)}$ data, it also could be used to separate particles within a PIV style device. One way to use APEP for a separation would be to separate based on differences in $\mu_{EP}^{(3)}$ using a long channel similar to a capillary electrophoresis (CE) device; where the multi particle solution would enter at one time and elude at differing times. The other method for APEP in a PIV style channel is to cause the particles to migrate in opposite directions by altering the signal to have a nonzero time averaged electric field. The method of using APEP to cause particles to migrate in different directions was initially tested using a 2 µm particle (green) and a 5.1 µm particle (red). The applied signal was rectangular with a positive voltage of 300 V being applied for 200 ms and a negative voltage of -600 V being applied for 105 ms. Because the time averaged electric field cubed was negative both particles experienced a net positive velocity due to nonlinear EP ($\mu_{EP}^{(3)}$ was negative for both particles). The time averaged electric field was also negative which, because μ_{EK} was positive for both particles, caused the particles to experience a net negative linear EK velocity. Using this signal, which was arrived at after some fine tuning, the large particles (5.1 µm red) moved forwards ~200 µm in 15 s while the small particles (2 µm green) moved backwards ~500 µm in 25 s (Fig. 23).
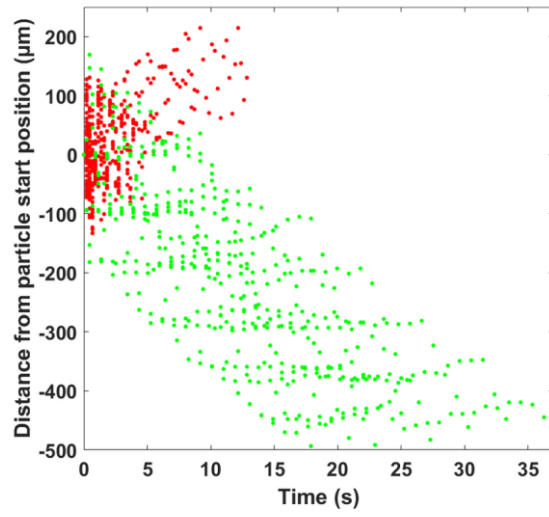
Figure 23: Plot of 5.1 µm particles in red and 2 µm particles in green over time with rectangular signal

applied. Applied signal consisted of 300 V being applied for 200 ms and -600 V being applied for 105 ms.

References

(1)   Schnitzer, O.; Zeyde, R.; Yavneh, I.; Yariv, E. *Phys. Fluids* **2013**, *25* (5). doi:10.1063/1.4804672

(2)   Fernandez, R. E.; Rohani, A.; Farmehini, V.; Swami, N. S. *Anal. Chim. Acta* **2017**, *966*, 11–33. doi:10.1016/j.aca.2017.02.024

(3)   Elitas, M.; Martinez-Duarte, R.; Dhar, N.; McKinney, J. D.; Renaud, P. *Lab Chip* **2014**, *14* (11), 1850–1857. doi:10.1039/c4lc00109e

(4)   Jung, B.; Zhu, Y.; Santiago, J. G. *Anal. Chem.* **2007**, *79* (1), 345–349. doi:10.1021/ac060949p

(5)   Ding, J.; Woolley, C.; Hayes, M. A. *Anal. Bioanal. Chem.* **2017**, *409* (27), 6405–6414. doi:10.1007/s00216-017-0582-5

(6)   Gadish, N.; Voldman, J. *Anal. Chem.* **2006**, *78* (22), 7870–7876. doi:10.1021/ac061170i

(7)   Issaq, H. J. *Electrophoresis* **2000**, *21* (10), 1921–1939. doi:10.1002/1522-2683(20000601)21:10<1921::AID-ELPS1921>3.0.CO;2-Y

(8)   Pethig, R. *J. Electrochem. Soc.* **2017**, *164* (5), B3049–B3055. doi:10.1149/2.0071705jes

(9)   Hoettges, K. F.; Henslee, E. A.; Torcal Serrano, R. M.; Jabr, R. I.; Abdallat, R. G.; Beale, A. D.; Waheed, A.; Camelliti, P.; Fry, C. H.; van der Veen, D. R.; Labeed, F. H.; Hughes, M. P. *Sci. Rep.* **2019**, *9* (1), 1–13. doi:10.1038/s41598-019-55579-9

(10)   Hughes, M. P. *Nanoelectromechanics in Engineering and Biology*; 2002.

doi:10.1201/9781315219202

(11)   Dukhin, S. S. *Adv. Colloid Interface Sci.* **1993**, *44* (C), 1–134. doi:10.1016/0001-
         8686(93)80021-3

(12)   Dukhin, S. S. *Adv. Colloid Interface Sci.* **1991**, *35* (C), 173–196. doi:10.1016/0001-
         8686(91)80022-C

(13)   Lapizco-Encinas, B. H. *RSC Detect. Sci.* **2015**, *2015-Janua* (5), 192–223

(14)   Coll De Peña, A.; Miller, A.; Lentz, C. J.; Hill, N.; Parthasarathy, A.; Hudson, A. O.;
         Lapizco-Encinas, B. H. *Anal. Bioanal. Chem.* **2020**. doi:10.1007/s00216-020-02621-9

(15)   Cardenas-benitez, B.; Lapizco-encinas, B. H.; Jind, B.; Gallo-villanueva, R. C.; Martinez-
         chapa, S. O.; Perez-gonzalez, V. H. **2020**

(16)   Jones, T. B. *Electromechanics of Particles*; Cambridge University Press, 1995.
         doi:10.1017/cbo9780511574498

(17)   Markx, G. H.; Huang, Y.; Zhou, X.-F.; Pethig, R. *Dielectrophoret Ic Characterization and
         Separation of Micro-Organisms*; 1994; Vol. 140

(18)   W. M. Arnold, H. P. Schwan, and U. Z. *J.Phys.Chem.* **1987**, No. 91, 5093–5098

(19)   Zhu, J.; Canter, R. C.; Keten, G.; Vedantam, P.; Tzeng, T. R. J.; Xuan, X. *Microfluid.
         Nanofluidics* **2011**, *11* (6), 743–752. doi:10.1007/s10404-011-0839-9

(20)   Zhu, J.; Xuan, X. *Electrophoresis* **2009**, *30* (15), 2668–2675. doi:10.1002/elps.200900017

(21)   Li, M.; Li, S.; Li, W.; Wen, W.; Alici, G. *AIP Conf. Proc.* **2013**, *1542* (2013), 1150–1153. doi:10.1063/1.4812140

(22)   Wang, Q.; Dingari, N. N.; Buie, C. R. *Electrophoresis* **2017**, *38* (20), 2576–2586. doi:10.1002/elps.201700144

(23)   Schnitzer, O.; Yariv, E. *Phys. Fluids* **2014**, *26* (12), 122002. doi:10.1063/1.4902331

(24)   Butt, H.-J.; Graf, K. (Karlheinz); Kappl, M. *Physics and Chemistry of Interfaces*; Wiley-VCH, 2003

(25)   Gencoglu, A.; Olney, D.; Lalonde, A.; Koppula, K. S.; Lapizco-Encinas, B. H. *Electrophoresis* **2014**, *35* (2–3), 362–373. doi:10.1002/elps.201300385

(26)   Luo, J.; Muratore, K. A.; Arriaga, E. A.; Ros, A. *Anal. Chem.* **2016**, *88* (11), 5920–5927. doi:10.1021/acs.analchem.6b00837

(27)   Kim, D.; Luo, J.; Arriaga, E. A.; Ros, A. *Anal. Chem.* **2018**, *90* (7), 4370–4379. doi:10.1021/acs.analchem.7b03774

(28)   Lentz, C. J.; Hidalgo-Caballero, S.; Lapizco-Encinas, B. H. *Biomicrofluidics* **2019**, *13* (4), 044114. doi:10.1063/1.5115153

(29)   Duffy DC; McDonald JC; Schueller OJA; Whitesides GM. *Anal. Chem.* **1998**, *70* (23), 4974–4984

(30)   Weiss, N. G.; Jones, P. V.; Mahanti, P.; Chen, K. P.; Taylor, T. J.; Hayes, M. A. *Electrophoresis* **2011**, *32* (17), 2292–2297. doi:10.1002/elps.201100034

(31)   Hidalgo-Caballero, S.; Lentz, C. J. C. J. C. J.; Lapizco-Encinas, B. H. B. H. *Electrophoresis* **2019**, *40* (10), 1395–1399. doi:10.1002/elps.201800425

(32)   Saucedo-Espinosa, M. A.; Lapizco-Encinas, B. H. *Biomicrofluidics* **2016**, *10* (3). doi:10.1063/1.4953183

(33)   Shimizu, M.; Okutomi, M. *Syst. Comput. Japan* **2003**, *34* (12), 1–10. doi:10.1002/scj.10506

(34)   Hill, N.; Lapizco-Encinas, B. H. *Electrophoresis* **2019**, 2541–2552. doi:10.1002/elps.201900177

(35)   Hossan, M. R.; Dillon, R.; Roy, A. K.; Dutta, P. *J. Colloid Interface Sci.* **2013**, *394* (1), 619–629. doi:10.1016/j.jcis.2012.12.039

(36)   Lapizco-Encinas, B. H. *Electrophoresis* **2019**, *40* (3), 358–375. doi:10.1002/elps.201800285

(37)   Sureda, M.; Miller, A.; Diez, F. J. *Electrophoresis* **2012**, *33* (17), 2759–2768. doi:10.1002/elps.201200202

(38)   Dukhin, A. S.; Dukhin, S. S. *Electrophoresis* **2005**, *26* (11), 2149–2153. doi:10.1002/elps.200410408